

Ultraviolet absorption cross sections of carbonyl sulfide isotopologues OC^{32}S , OC^{33}S , OC^{34}S and O^{13}CS : isotopic fractionation in photolysis and atmospheric implications

S. Hattori¹, S. O. Danielache¹, M. S. Johnson², J. A. Schmidt², H. G. Kjaergaard², S. Toyoda³, Y. Ueno⁴, and N. Yoshida^{1,3}

¹Department of Environmental Science and Technology, Interdisciplinary Graduate School of Science and Engineering, Tokyo Institute of Technology, Yokohama, 226-8502, Japan

²Copenhagen Center for Atmospheric Research, Department of Chemistry, University of Copenhagen, Universitetsparken 5, 2100 Copenhagen, Denmark

³Department of Environmental Chemistry and Engineering, Interdisciplinary Graduate School of Science and Engineering, Tokyo Institute of Technology, Yokohama, 226-8502, Japan

⁴Department of Earth and Planetary Science, Tokyo Institute of Technology, Meguro-ku, Tokyo, 152-8551, Japan

Received: 6 July 2011 – Published in Atmos. Chem. Phys. Discuss.: 19 July 2011

Revised: 3 October 2011 – Accepted: 5 October 2011 – Published: 14 October 2011

Abstract. We report measurements of the ultraviolet absorption cross sections of OC^{32}S , OC^{33}S , OC^{34}S and O^{13}CS from 195 to 260 nm. The OCS isotopologues were synthesized from isotopically-enriched elemental sulfur by reaction with carbon monoxide. The measured cross section of OC^{32}S is consistent with literature spectra recorded using natural abundance samples. Relative to the spectrum of the most abundant isotopologue, substitution of heavier rare isotopes has two effects. First, as predicted by the reflection principle, the Gaussian-based absorption envelope becomes slightly narrower and blue-shifted. Second, as predicted by Franck-Condon considerations, the weak vibrational structure is red-shifted. Sulfur isotopic fractionation constants ($^{33}\epsilon$, $^{34}\epsilon$) as a function of wavelength are not highly structured, and tend to be close to zero on average on the high energy side and negative on the low energy side. The integrated photolysis rate of each isotopologue at 20 km, the approximate altitude at which most OCS photolysis occurs, was calculated. Sulfur isotopic fractionation constants at 20 km altitude are $(-3.7 \pm 4.5)\text{‰}$ and $(1.1 \pm 4.2)\text{‰}$ for $^{33}\epsilon$ and $^{34}\epsilon$, respectively, which is inconsistent with the previously estimated large fractionation of over 73‰ in $^{34}\epsilon$. This demonstrates that OCS photolysis does not produce sulfur isotopic fractionation of more than ca. 5‰, suggesting OCS may indeed be a significant source of background strato-

spheric sulfate aerosols. Finally, the predicted isotopic fractionation constant for ^{33}S excess (^{33}E) in OCS photolysis is $(-4.2 \pm 6.6)\text{‰}$, and thus photolysis of OCS is not expected to be the source of the non-mass-dependent signature observed in modern and Archaean samples.

1 Introduction

The stratospheric sulfate aerosol (SSA) layer plays an important role for Earth's radiation budget and modulates the concentration of stratospheric ozone due to surface heterogeneous reactions (Junge, 1966; Myhre et al., 2004; Mills et al., 2005). Sulfur compounds from volcanic eruptions such as Mt. Agung (1963) and Mt. Pinatubo (1992) produce large amounts of SSA. However, SSA persists even in the absence of volcanic input indicating a background source (Crutzen, 1976; Hofmann, 1990). Carbonyl sulfide (OCS) is the most abundant sulfur containing gas in the atmosphere, with an average mole fraction of 0.5×10^{-9} throughout the troposphere (Watts, 2000; Notholt et al., 2003). Since the discovery of SSA (Junge and Manson, 1961), the photolysis of OCS was thought to be a significant source because it is transported into the stratosphere where it is broken down by photolysis and radical reactions with OH and $\text{O}(^3\text{P})$. Chin and Davis (1995) used a 1-D model to show that atmospheric OCS is inadequate to maintain the background SSA concentration; other significant of SSA sources including deep

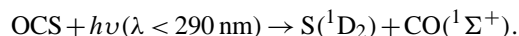


Correspondence to: S. Hattori
(hattori.s.ab@m.titech.ac.jp)

convection of SO₂ from the lower troposphere (Weissenstein et al., 1997; Kjellström, 1998; Pitari et al., 2002; Stevenson et al., 2003) and an in situ sulfuric acid photolysis and sulfur dioxide oxidation process (Mills et al., 2005) have been proposed. In contrast Barkley et al. (2008) found the stratospheric lifetime of OCS to be 64 ± 21 a from ACE satellite measurements, corresponding to a stratospheric sink of $63\text{--}124 \text{ Gg S a}^{-1}$, which matches the source needed to sustain the SSA production of $30\text{--}170 \text{ Gg S a}^{-1}$ (Chin and Davis, 1995). The background source of SSA is not known with any certainty.

Isotopic analysis is used to trace the sources and transformations of atmospheric trace gases (e.g. Krouse and Grinenko, 1991; Johnson et al., 2002; Brenninkmeijer et al., 2003). The observed isotopic composition of a species and chemical isotopic fractionations are linked to its sources by the mass balance equation. In addition to ³⁴S/³²S ratios, non-mass-dependent sulfur isotopic compositions have been found in the Archean rock record, Martian meteorites, and sulfate aerosols (Farquhar et al., 2000; Baroni et al., 2007, 2008). The $\delta^{34}\text{S}$ value of tropospheric OCS has not been measured but was estimated to be 11 ‰ (Krouse and Grinenko, 1991). Concentration profiles of OC³⁴S and OC³²S retrieved from infrared limb transmittance spectra acquired by the JPL MkIV instrument indicated an extremely large photochemical fractionation ($(73.8 \pm 8.6) \%$; Leung et al., 2002). This isotopic fractionation is not consistent with the one known measurement of $\delta^{34}\text{S}$ in SSA (2.6 ‰; Castleman et al., 1974). In contrast, Lin et al. (2011) recently reported relatively small fractionation in the range of -10.5 to $+5.3 \%$ in ³⁴S in laboratory photolysis of OCS suggesting the possibility that OCS may be a viable source of SSA. Modeling shows that while reactions with OH and O(³P) are important for removing OCS in the lower stratosphere, photolysis is the dominant loss process above 14 km, accounting for over 80 % of the chemical sink above 20 km (Danielache et al., 2008b). Therefore, we have focused on sulfur isotopic fractionation in OCS photolysis in this study.

Like carbon dioxide (CO₂) and nitrous oxide (N₂O), OCS is a linear 16 valence electron atmospheric trace gas with forbidden electronic transitions that become allowed as the molecule bends (Suzuki et al., 1998):



The excited state potential energy surface imparts a strong torque on the system producing a highly rotationally excited CO fragment and trapping trajectories on the repulsive excited state potential energy surface long enough to give weak vibrational structure. Since the photolysis quantum yield is unity from 200 to 300 nm (Rudolph and Inn, 1981), the absorption spectrum of OCS can be used to calculate its photolysis rate. Isotopic substitution results in shifts in the absorption spectra of the substituted species; in the atmosphere this results in fractionation because the photolysis rate is dependent on the convolution of the actinic flux with the absorp-

tion cross section (Jørgensen et al., 2008). For example, the absorption cross sections of N₂O isotopomers and isotopologues (von Hessberg et al., 2004) and SO₂ isotopologues (Danielache et al., 2008a) have been investigated and demonstrate that photodissociation results in non-mass-dependent isotopic fractionation. In previous studies the absorption cross sections of commercial OC³⁴S and natural abundance OCS were measured to determine isotopic fractionation as a function of wavelength (Colussi et al., 2004), and theoretical calculations of OCS isotopologue cross sections have been made (Danielache et al., 2009). The former study reported that OC³⁴S has a stronger absorption than natural abundance OCS resulting in a large positive isotopic fractionation. The latter work reported significantly smaller isotopic fractionations than that of former study. Similarly, in a recent laboratory photolysis study of OCS, Lin et al. (2011) observed relatively small sulfur isotopic fractionation. The ultimate goal of the different approaches is the same: to investigate the sulfur isotope effect on OCS photolysis. Current theoretical methods (Danielache et al., 2009), however, are not precise enough to reconstruct the weak vibrational structures and magnitude of the absorption cross section. For laboratory experiments of OCS photolysis (Lin et al., 2011), the precision of the measurement is better than other approaches but the light source does not duplicate the stratospheric actinic flux. Therefore, one objective of this study is to make sense of sulfur isotopic fractionation using laboratory absorption cross section measurements. For this purpose, we synthesized the sulfur isotopologues of OCS using the same carbon monoxide material to isolate the effect of ¹³C, ¹⁸O and ¹⁷O isotope substitution.

Here, we present the UV absorption cross sections of isotopically substituted OCS (OC³²S, OC³³S, OC³⁴S, and O¹³CS) in the 195–260 nm region. Isotopic fractionation constants in photolysis as a function of wavelength for sulfur and carbon isotopes are calculated, and implications for atmospheric chemistry are discussed.

2 Experimental sections

2.1 Synthesis of OCS isotopologues and purification

The OCS isotopologues OC³²S, OC³³S, and OC³⁴S were synthesized by chemical conversion according to Ferm (1957). This procedure involved the reaction of carbon monoxide (CO) (Japan Fine Products, 99.99 % purity) with 1–5 mg of ³²S (99.99 % isotopic enrichment), ³³S (99.8 % isotopic enrichment) and ³⁴S (99.9 % isotopic enrichment) powders (Isoflex, USA). The elemental sulfur powders were put in Pyrex glass tubes (i.d. 9 mm) and the air was evacuated. After evacuation, a stoichiometric excess of CO (2 to 3 times) was added and the tubes were sealed. The samples were heated at 573 K for 24 h, converting S into OCS.

The product was expected to include impurities such as CO, CO₂, hydrogen sulfide (H₂S) and carbon disulfide (CS₂). In particular, CS₂ has an intense overlapping UV absorption in the region 190–212 nm that is ca. 20 000 times larger than that of OCS (Molina et al., 1981). The samples were purified using a gas chromatograph (GC) equipped with a thermal conductivity detector (TCD) (GC-14B; Shimadzu, Kyoto, Japan) and packed column (Pora Pack Q, 2 mm i.d., 2.4 m) maintained at 333 K. Ultra-pure He (Japan Air Gases, >99.99995 % purity) was used as the carrier gas at a flow rate of 25 ml min⁻¹. The GC oven temperature program was 333 K for 8 min, increased from 333 to 473 K at a rate of 25 K min⁻¹, and then held at 473 K for 2 min. OCS with a retention time of ca. 5.2 min was trapped at liquid nitrogen temperature (77 K) after the GC. The GC column was carefully baked between the samples to avoid contamination from other isotopologues and other components. The retention times of impurities were 3.0 min, 4.0 min and 12.0 min for CO₂, H₂S and CS₂, respectively. Reanalysis of the purified OCS sample confirmed that these impurities were below the detection limit (<0.1 %). Purified OCS was transferred into evacuated glass tubes and stored in the dark at room temperature before experiments. The recovery of OCS was 70–80 % and the same CO sample was used to synthesize OC³²S, OC³³S and OC³⁴S. Since the method does not involve sulfur other than the reagent, isotopic contamination of the samples was negligible as verified with infrared spectroscopy (Bruker IFS 66 V/s).

For ¹³C-enriched OCS, commercial O¹³CS (Icon stable isotopes, ¹³C 99 % purity) was used. Since the O¹³CS sample was assumed to include impurities such as CS₂ and CO₂, the commercial sample was also purified according to procedure described above.

2.2 Spectroscopy

Like N₂O, OCS is photolyzed in the stratospheric UV window. This window coincides with the low energy shoulder of the N₂O absorption cross section, which is sensitive to temperature. However, in the case of OCS, the stratospheric UV window coincides with the high energy side of the absorption cross section which is only weakly sensitive to temperature. Room temperature measurements are therefore adequate as a first approximation.

Spectra were recorded at (295 ± 1) K using a UV/Vis dual-beam photo spectrometer (Lambda 1050 NB; Perkin Elmer Inc., USA) equipped with deuterium lamp, using a 10.00 cm long cell with CaF₂ windows. The spectral resolution was set to 0.1 nm and data were recorded at 0.02 nm (2.96 to 5.26 cm⁻¹) intervals. Sample pressures were measured using a 133 mbar range capacitance manometer (0.15 % precision; Edwards Inc. UK) calibrated to the Danish national standard. Absorptivities were derived using the measured spectrum of the empty cell and of the cell including sample. Background, sample and a second background spectrum were measured in

sequence to correct for possible drifts in the system, e.g. lamp intensity and detector and electronics sensitivity. One measurement took approximately 50 min and three to four repetitions of measurements of a single OCS isotopologues were carried out in a day. After evacuation of the gas line and the cell during the night, the next isotopologue measurement was carried out. The measurements for the OCS isotopologues were carried out over a continuous series of days. Wavelength was calibrated internally using the Shumann-Runge bands of O₂ present in the spectrometer. Sample pressures ranged from 8 to 23 mbar. In this range, we confirmed that the cross section values were independent of gas pressure. Measurement sequences were performed 10 times, 6 times, 6 times, and 6 times for OC³²S, OC³³S, OC³⁴S, and O¹³CS, respectively.

The measured intensities were converted to absorption cross sections, $\sigma(\lambda)$, using the Beer-Lambert law:

$$\sigma(\lambda) = \frac{1}{Nl} \ln \left[\frac{I_0(\lambda)}{I(\lambda)} \right], \quad (1)$$

where N is the OCS number density, l is the path length of the cell, $I(\lambda)$ is the intensity as a function of wavelength through cell with sample, and $I_0(\lambda)$ is the intensity through the evacuated cell. $I_0(\lambda)$ values were taken as the average of intensities measured before and after sample intensities.

2.3 Notations

2.3.1 Wavelength dependent of isotopic fractionations

In order to describe the change of cross section for heavier isotopologues the isotopic fractionation factor (α) as a function of wavelength (λ /nm) was investigated. However, the samples used in this study contained small isotopic impurities. The effect of the impurities was corrected using the isotopic purities provided by the manufacturer (see Appendix). Since the isotopic fractionation factors (α) are generally close to unity, it is common to quantify the isotope effect in terms of the fractionation constant (ϵ) and ϵ is often given in per mil notation (‰). In this study ϵ for sulfur and carbon isotopes are described using Eqs. (2) and (3),

$${}^x\epsilon(\lambda) = \frac{{}^x\sigma(\lambda)}{{}^{32}\sigma(\lambda)} - 1 \quad (x = 33 \text{ or } 34) \quad (2)$$

$${}^{13}\epsilon(\lambda) = \frac{{}^{13}\sigma(\lambda)}{{}^{12}\sigma(\lambda)} - 1, \quad (3)$$

where ${}^{32}\sigma$, ${}^x\sigma$, ${}^{12}\sigma$ and ${}^{13}\sigma$ are the absorption cross section of OC³²S, OC³³S or OC³⁴S, O¹²CS and O¹³CS, respectively. Non-mass-dependent fractionation is often described as deviation from mass-dependent fractionation law using Eq. (4).

$${}^{33}E(\lambda) = {}^{33}\epsilon(\lambda) - \left[\left({}^{34}\epsilon(\lambda) + 1 \right)^{0.515} - 1 \right] \quad (4)$$

2.3.2 Isotopic fractionation constants of OCS photolysis at 20 km altitude

From the measured absorption cross sections of the different isotopologues, it is possible to compute an effective fractionation constant for solar photolysis in the lower stratosphere. The photolysis rates constants (J) can be evaluated using Eq. (5).

$${}^x J = \int_{\lambda_1}^{\lambda_2} I(\lambda) {}^x \sigma(\lambda) \varphi(\lambda) d\lambda, \quad (5)$$

where φ is the quantum yield of OCS photolysis which is assumed to be 1 for all isotopologues, and the index x represents the isotopologue. In order to investigate the fractionation of each isotopologue relative to OC^{32}S in the OCS photolysis region, the actinic flux at 20 km altitude was used as I from 195–260 nm. This actinic flux was provided by Chris McLinden of Meteorological Service of Canada (McLinden et al., 2002).

Actual fractionation constants can be calculated using Eqs. (6) and (7).

$${}^x \varepsilon = \frac{{}^x J}{{}^{32} J} - 1 \quad (x = 33 \text{ or } 34) \quad (6)$$

$${}^{13} \varepsilon = \frac{{}^{13} J}{{}^{12} J} - 1 \quad (7)$$

The mass-dependent relationship describing the equilibrium distribution of three sulfur isotopes between phases has been established by Hulston and Thode (1965) as following Eq. (8).

$${}^{33} \alpha = {}^{34} \alpha^{0.515} \quad (8)$$

Finally we approximate deviation from mass-dependent fractionation in ${}^{33}\text{S}$ (${}^{33}E$) according to Ueno et al. (2009).

$${}^{33} E = {}^{33} \varepsilon - \left[\left({}^{34} \varepsilon + 1 \right)^{0.515} - 1 \right] \approx {}^{33} \varepsilon - 0.515 {}^{34} \varepsilon \quad (9)$$

2.3.3 Sulfur isotopic compositions

Although carbon isotope ratios in OCS have not been reported, sulfur isotope ratios and fractionations in OCS and its related compounds have been considered in several studies. Here, sulfur isotopic compositions are reported as

$$\delta^x \text{S} = \frac{{}^x R_{\text{sample}}}{{}^x R_{\text{standard}}} - 1, \quad (10)$$

where x represents 33 or 34 and R denotes the isotope ratios (${}^{33}/{}^{34}\text{S}/{}^{32}\text{S}$) of samples and standards. Isotope ratios of sulfur are reported relative to the Vienna Canyon Diablo Troilite (VCDT) standard and often denoted in per mil (‰).

In addition to $\delta^{34}\text{S}$ values, non-mass-dependent fractionation in sulfur is an important quantity. The capital delta

notation ($\Delta^{33}\text{S}$) is used to describe and distinguish between mass-dependent and non-mass-dependent isotopic compositions, where

$$\Delta^{33}\text{S} = \delta^{33}\text{S} - \left[\left(\delta^{34}\text{S} + 1 \right)^{0.515} - 1 \right]. \quad (11)$$

This notation describes the excess or deficiency of ${}^{33}\text{S}$ relative to a reference “mass-dependent” fractionation array.

3 Results and discussion

3.1 Error budget

Errors in the absorption cross sections come from several sources. Some error is due to random variation in the spectrometer (detector and amplifier sensitivity, lamp stability etc.). Error in sample density arises from the precision of the pressure gauges ($\pm 0.15\%$ according to the manufacturer). Measurements used the same cell (path length 10.00 cm) and the temperature of the laboratory was (295 ± 1) K; overall, error due to measurement of pressure was less than 0.4%. These errors were propagated and included standard deviations as shown in Fig. 2a–c. The average relative standard deviations (RSD; %) in the 195–260 nm region for OC^{32}S , OC^{33}S , OC^{34}S and O^{13}CS are 2.4%, 2.3%, 2.2% and 3.1%, respectively. In the high absorbance region (210 to 235 nm) RSDs are less than 0.5%. The isotopologues RSDs as a function of wavelength are shown in Fig. A1 of the Supplement.

Sample purity may result in systematic error independent of the number of measurements. After the purification detailed above we evaluated sample purity using FTIR spectroscopy, similar to the method of Danielache et al. (2008a). The concentrations of infrared active impurities were determined from the IR spectra using the global nonlinear least squares spectral fitting procedure developed by Griffith (1996). Line parameters were taken from the HITRAN database (Rothman et al., 2005). The samples used in this study contain CO_2 at mole fractions of 0.04%, 0.04%, 0.03%, and 0.04% for OC^{32}S , OC^{33}S , OC^{34}S and O^{13}CS , respectively; other impurities could not be detected.

3.2 Comparison with previous studies

The absorption cross section of OC^{32}S is shown in Fig. 1. Vibrational structure can be seen superimposed on a broad Gaussian-like absorption band typical of direct dissociation. The measured absorption cross section of OC^{32}S is consistent with previous studies using natural abundance OCS samples such as Molina et al. (1981) and Wu et al. (1999) (Fig. 1). In particular, the difference between the present study and the data of Wu et al. (1999) was less than 1% in the high absorption region (210–230 nm). Despite the lower spectral resolution of our study in comparison with Wu et al. (1999), the vibrational structure was resolved and reproduced (Fig. 1). At wavelengths shorter than 210 nm, the cross

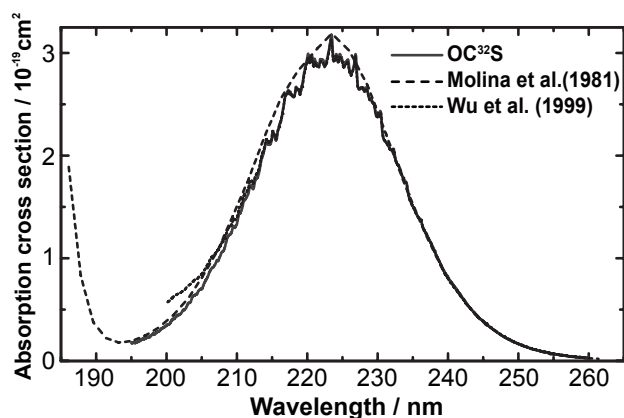


Fig. 1. Measured absorption cross section of the OC³²S isotopologue compared to the spectra of natural isotopic abundance samples measured by Molina et al. (1981) (long dashed line) and Wu et al. (1999) (short dashed line) in the region of 190–260 nm.

sections of Wu et al. (1999) are larger than those of OC³²S in this study, but this difference is due to their sample's contamination by CS₂ as discussed in Wu et al. (1999).

3.3 Comparisons of absorption of cross sections of OCS isotopologues

The isotopologue's absorption cross sections are shown in Fig. 2. While similar structures are observed for OC³²S, OC³³S, and OC³⁴S, O¹³CS has a slightly different structure. Peak positions vary systematically from OC³²S, OC³³S, OC³⁴S to O¹³CS, the shift being approximately linear in transition energy (Fig. 3). A similar pattern of shifting was observed for SO₂ isotopologues (Danielache et al., 2008a) and N₂O isotopomers and isotopologues (Selwyn and Johnston, 1981; Schmidt et al., 2011). The maximum in the absorption cross sections, σ_{\max} , occurs at 223.44 nm, 223.50 nm, 223.54 nm, and 223.54 nm for OC³²S, OC³³S, OC³⁴S, and O¹³CS, respectively (Table 1).

It is noteworthy that the largest changes in integrated intensity, width of absorption envelope and shift in position of vibrational structure was seen for ¹³C which is expected based on the change in the ground state vibrational wavefunction (Danielache et al., 2009) and comparison to N₂O (Johnson et al., 2001). In both molecules the transition is forbidden when the molecule is linear, and becomes allowed as the system bends. As a result there is an unusually large increase in the transition intensity with bending excitation. Substitution at the carbon atom changes the degree of bending excursion much more than sulfur substitution, resulting in weaker intensity across the band.

We compare our OC³²S and OC³⁴S cross sections with those of Colussi et al. (2004). Although the red-shift of σ_{\max} for OC³⁴S relative to OC³²S is consistent with this work, the reported σ absorption intensity of OC³⁴S relative

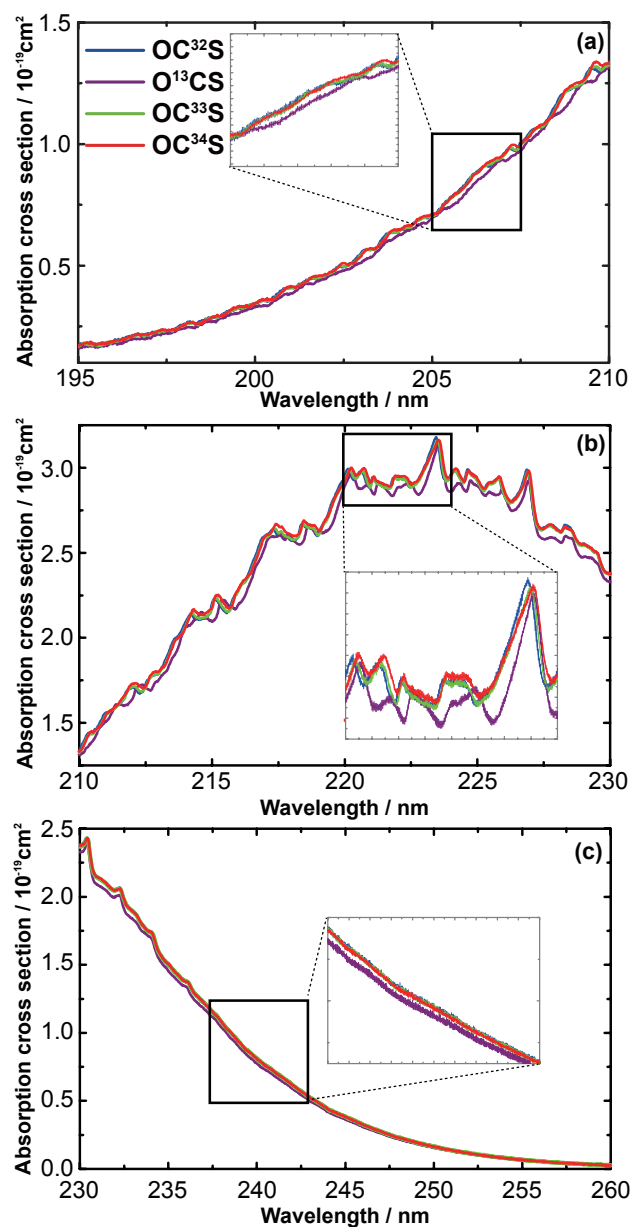


Fig. 2. Comparison of absorption cross sections measured at 0.1 nm resolution and 0.02 nm step size for isotopically enriched samples of OC³²S, OC³³S, OC³⁴S, and O¹³CS divided in three energy ranges; 195–210 nm (a), 210–230 nm (b) and 230–260 nm (c).

to OC³²S is opposite to the results of this study. Colussi et al. (2004) compared the spectrum of natural abundance OCS (about 90 %) and commercial OC³⁴S after distillation using an Hg(II)SO₄ solution, and their sample of OC³⁴S contained about 30 % CO₂. This level of impurity likely affected the determination of the absolute cross sections; we note that the absolute cross section of their natural abundance sample is about 10 % larger than the cross section reported by Wu et al. (1999). As presented above, our samples were

carefully purified and the impurities were documented by several methods. In addition to the absence of impurities in the samples in the present study, the carbon and oxygen isotopic purity is the same for OC^{32}S , OC^{33}S and OC^{34}S . Colussi et al. (2004) predict a large photolytic isotopic fractionation of sulfur and this is not consistent with our result.

3.4 Shifted spectra of OCS isotopologues

The positions of the vibrational peaks of the heavier isotopologues (OC^{33}S , OC^{34}S and O^{13}CS) were generally red-shifted relative to the most abundant species (OC^{32}S) cf. Fig. 3. This red-shift in vibrational structure for heavier isotopologues is consistent with a Franck-Condon model in which isotopic substitution changes the positions of the vibrational levels of the ground and excited electronic states. At the lowest transition energies the zero point energy (ZPE) shift of the ground state is larger than the shift in the excited state. With increasing energy transitions are made to upper state levels with increasing vibrational excitation. For these states the isotope shift in frequency is larger than the change in the ground state, leading to red-shifting of the vibrational structure extending over most of the band. The exact position of the absorption maximum (Fig. 2) is due to a vibrational peak, and so the position of the maximum in Table 1 is red shifted for isotopic substitution.

For direct photodissociation, the absorption cross section is often fairly well approximated as an energy weighted Gaussian function. The reflection principle states that the absorption spectrum can be approximated by reflecting the initial vibrational wavefunction onto the energy axis across the repulsive excited state surface (Schinke, 1993). Energy weighted Gaussian functions (Eq. 12) were fitted to the isotopologue cross sections in order to discuss changes in the overall shape of the band.

$$\sigma(E_{\text{ph}}) = \left(\frac{\sigma_{\text{max}}}{E_{\text{max}}} \right) E_{\text{ph}} \exp\left[-w(E_{\text{max}} - E_{\text{ph}})^2\right], \quad (12)$$

where E_{max} indicates the wavenumber of σ_{max} , E_{ph} is the photon energy, and w is a width parameter. Plots of $\ln(\sigma(E_{\text{ph}})/E_{\text{ph}})$ vs. E_{ph} in the high absorbance region (210–235 nm) show the center (Center) and the full width at half maximum (FWHM) of the fitted spectra as summarized in Table 2. This shows that the heavy isotopologue band centers are blue-shifted, in accordance with the prediction of the reflection principle and the ZPE theory (Miller and Yung, 2000). In addition, the width (FWHM) is more narrow for the heavy isotopes as predicted by Liang et al. (2004). This is also expected since, for direct dissociation, the width of the cross section is proportional to width of the ground state vibrational wavefunction (Schinke, 1993). Consequently, the isotope effect on the UV absorption cross sections of OCS isotopologues is seen to arise from three effects: blue-shifting and a more narrow overall band for heavier isotopologues, and red-shifting of the weak vibrational structure for heavier isotopologues.

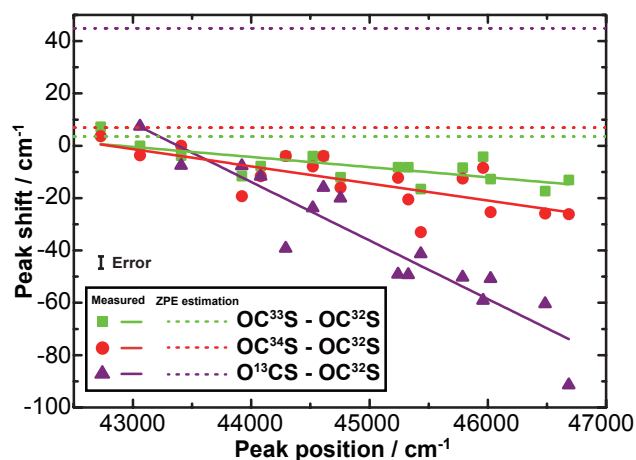


Fig. 3. Isotopic shift for the 210–230 nm region. The shift in the position of vibrational structure for the OC^{33}S , OC^{34}S , and O^{13}CS isotopologues relative to OC^{32}S are shown. Dotted line shows shifts using the ΔZPE model calculated in Danielache et al. (2009).

logues, and red-shifting of the weak vibrational structure for heavier isotopologues.

3.5 Integrated absorption cross sections

Integrated absorption cross sections for the 195–260 nm band vary with isotopic substitution (Table 1). In order to determine the fractionation constants from the measured cross section as described in next section, it is important to accurately determine the overall magnitude of the individual cross sections. This in turn, requires pure samples and an accurate determination of the pressure in the cell. To estimate the reliability of the magnitudes of the measured cross sections we compare the experimental integrated $\sigma(E_{\text{ph}})/E_{\text{ph}}$ with theoretical results.

The theoretical results are obtained using a recent ground state potential energy surface and transition dipole moments (Danielache et al., 2009).

The integrated intensity, s , is calculated using

$$s = \int_0^{\infty} \sigma(E_{\text{ph}}) E_{\text{ph}}^{-1} dE_{\text{ph}}. \quad (13)$$

The quantity s can also be obtained from the following expression (Schinke, 1993):

$$s = C \sum_i W_i \int |\Psi_i(\mathbf{R}) \mu_{\text{FI}}(\mathbf{R})|^2 d\mathbf{R}, \quad (14)$$

where \mathbf{R} are the nuclear coordinates, Ψ_i is the i -th vibrational wavefunction in the electronic ground state, μ_{FI} is the

Table 1. Wavelength at σ_{\max} , shifting of σ_{\max} , σ_{\max} ratio for each isotopologue, and the ratio of the areas under spectral curve for the measured spectra (195–260 nm). All comparisons are relative to OC³²S.

Isotopologues	λ at σ_{\max} (nm)	$\Delta\lambda$ of σ_{\max} (nm)	σ_{\max} ratio	Integrated absorption cross section relative to OC ³² S	
				Experiment	Theory
OC ³² S	223.44			1	1
OC ³³ S	223.50	0.06	0.993	0.997	0.9994
OC ³⁴ S	223.54	0.10	0.995	1.001	0.9989
O ¹³ CS	223.54	0.10	0.989	0.975	n.d.*

* n.d. = not determined

Table 2. Reconstructions of absorption cross sections of OCS isotopologues using Gaussian fitting.

	OC ³² S	OC ³³ S	OC ³⁴ S	O ¹³ CS
Center (nm)	223.165	223.163	223.143	223.105
FWHM* (nm)	24.958	24.915	24.865	24.713

* Full width at half maximum.

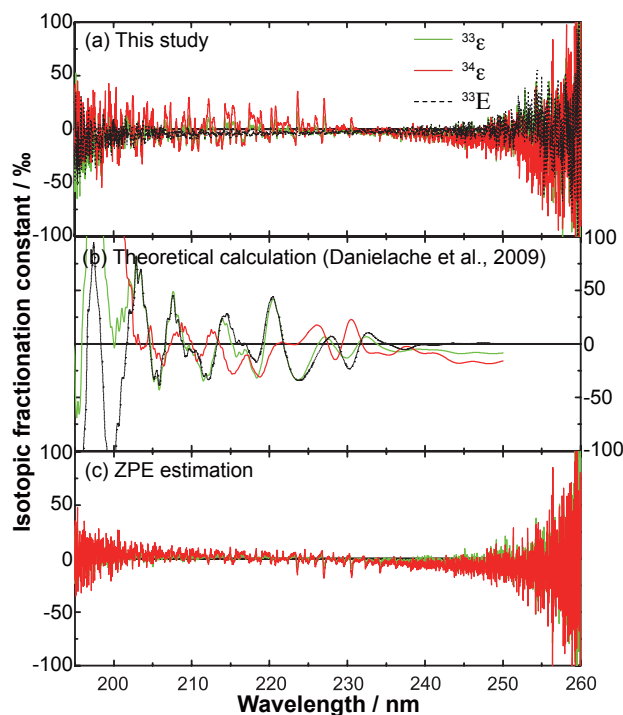
transition dipole moment, C is a universal constant and W_i is the Boltzmann weighting factor,

$$W_i = d_i \exp\left(\frac{-E_i}{k_b T}\right) \left[\sum_j d_j \exp\left(\frac{-E_j}{k_b T}\right) \right]^{-1} \quad (15)$$

where d_i is the degeneracy of state i . Only the vibrational ground state and first excited bending and stretching states were considered. Table 1 shows integrated energy weighted cross sections relative to the most abundant isotopologue. The relative integrated absorption cross section measurements are in excellent agreement with theory, showing deviations of less than 0.3%. The differences are due to several factors. One is the difficulty of accurately predicting transition intensities within quantum chemical methods. In addition there are systematic errors in the measurement as described above.

3.6 Isotopic fractionation constants for OCS photolysis

Using Eqs. (2–4), wavelength dependent isotopic fractionation constants were calculated and are presented in Fig. 4 for sulfur isotopes and Fig. 5 for carbon isotopes. Since OCS does not have a highly structured absorption, the isotopic fractionation constant does not show the highly structured fractionation spectrum seen for SO₂ isotopologues which varies from -1000‰ to $+1000\text{‰}$ (Danielache et al., 2008a). It is worth noting that the large variation in the isotopic fractionation at low and high energies may be due to measurement errors occurring at regions of low absorptivity (Figs. 4

**Fig. 4.** Isotopic fractionation constants for sulfur species (^{33/34} $\epsilon(\lambda)$) and for ³³S excess (³³ $E(\lambda)$) plotted as a function of wavelength; this study (a), theoretical calculation (Danielache et al., 2009) (b), ZPE estimation (Miller and Yung, 2000; Danielache et al., 2009) (c).

and 5), but the trend of the wavelength dependence of isotopic fractionation can be seen. Generally it is close to zero on average on the higher energy side (195–230 nm) in both ³³ ϵ and ³⁴ ϵ . In contrast, on the lower energy side, negative fractionation constants are observed that are in good agreement with the ZPE estimation and Danielache et al. (2009) (Fig. 4). In contrast, ¹³ ϵ on the higher energy side was lower than that of the ZPE estimation, suggesting the effect of narrowing is dominant in this region (Fig. 5).

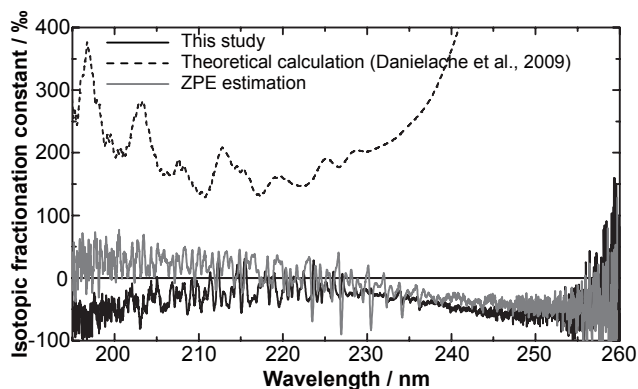


Fig. 5. Carbon isotope fractionation constant ($^{13}\epsilon(\lambda)$) calculated from Eq. (6) as a function of wavelength. Black line: this study; black dotted line: theoretical calculation (Danielache et al., 2009); gray line: ZPE estimation (Miller and Yung, 2000; Danielache et al., 2009).

3.7 Atmospheric implications

3.7.1 Prediction of sulfur isotopic fractionation of OCS photolysis in the modern atmosphere

The calculated value of $I(\lambda)^{32}\sigma(\lambda)\varphi(\lambda)$ shows a maximum at 210–211 nm (Fig. 6). This finding is largely consistent with previous work by Colussi et al. (2004) which found the maximum of $I(\lambda)^{32}\sigma(\lambda)$ at approximately 209 nm. Calculated $^{32/33/34/13}J$ values and estimated fractionation constants ($^{33}\epsilon$, $^{34}\epsilon$ and $^{13}\epsilon$) at 20 km altitude are summarized in Table 3. The estimated ^{32}J is approximately 1.3×10^{-8} molecule s^{-1} , being of the same order as a previous estimate (Chin and Davis, 1995). As described above, our measurements have not only random errors but also systematic errors. Therefore, as a total estimated error, we propagate a standard deviation from repeated measurements and a systematic error of 3 ‰ which is estimated from the differences between integrated cross sections and theory. The predicted isotopic fractionation constants in OCS photolysis at 20 km altitude are $(-3.7 \pm 4.5)\%$, $(1.1 \pm 4.2)\%$, $(-26.8 \pm 4.3)\%$, and $(-4.2 \pm 6.6)\%$ for $^{33}\epsilon$, $^{34}\epsilon$, $^{13}\epsilon$ and ^{33}E , respectively (Table 3).

This $^{34}\epsilon$ is inconsistent with the observed isotopic fractionation in ^{34}S of $(73.8 \pm 8.6)\%$ in OCS decomposition for the lower stratosphere derived using stratospheric OC^{34}S and OC^{32}S concentration profiles from the infrared limb transmittance spectra acquired by the JPL MkIV instrument (Leung et al., 2002). First, consider that the sulfur isotopic fractionation in ^{34}S of 73.8 ‰ may not be due to OCS photolysis as a significant amount of OCS is removed by radical reactions. However the $^{34}\epsilon$ of $\text{OCS} + \text{OH}$ is estimated to be small (-2.56% ; Danielache et al., 2008). Further, the apparent fractionation derived from concentration profiles is usually about half of the process fractionation constant due to mixing

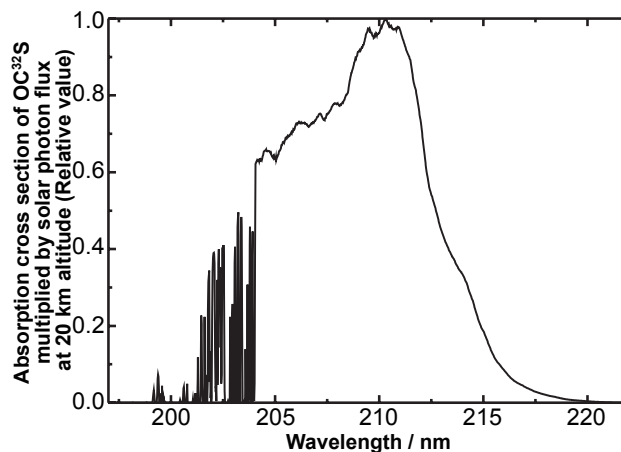


Fig. 6. Photolysis rates as a function of wavelength for OC^{32}S at 20 km in arbitrary units.

(McLinden et al., 2003), so the isotopic fractionation in ^{34}S of $(73.8 \pm 8.6)\%$ from the MkIV instrument analysis (Leung et al., 2002) does not match the previously estimated isotopic fractionation in OCS photolysis in ^{34}S of $(67 \pm 7)\%$ (Colussi et al., 2004). One concern is that these retrievals are difficult and have yet to be confirmed in other studies (either via remote sensing or sampling). We conclude that further observations are required to confirm or disprove the observed OCS isotopologues profiles reported by Leung et al. (2002).

3.7.2 OCS as a candidate of background SSA sulfur origin

$\delta^{34}\text{S}$ values of 11 ‰ in tropospheric OCS were estimated by mass balance of oceanic sulfur and terrestrial sulfur (Krouse and Grinenko, 1991). The OCS oxidation product, background SSA, is reported to be 2.6 ‰ (Castleman et al., 1974), indicating that background SSA is less enriched in ^{34}S than tropospheric OCS. Our results show that OCS photolysis gives only a small isotopic fractionation of $^{34}\epsilon$ ($(1.1 \pm 4.2)\%$) and Danielache et al. (2008b) reported that the OCS reaction with OH also has a small and negative $^{34}\epsilon$ (-2.56%). Consequently, sulfate from OCS sink reactions will not be fractionated more than 5 ‰ compared to the initial material, showing that OCS is an acceptable source of background SSA.

Recently Lin et al. (2011) reported the results of laboratory experiments on OCS. They found that small values of $^{34}\epsilon$ (-10.5 to $+5.3\%$) in $\lambda > 280$ nm experiments is consistent with the ZPE fractionation estimate. Their negative values of $^{34}\epsilon$ on the low energy side ($\lambda > 230$ nm) due to the ZPE shift of heavier sulfur isotopologues are largely consistent with this study (Fig. 4), although it is noteworthy that UV light from 205 to 215 nm is predicted to be most important for OCS photolysis in the modern atmosphere (Fig. 6). In addition, recently, the sulfur isotopic

Table 3. Photolysis rate of each OCS isotopologues at 20 km altitude ($^{32/33/34/13}J$) and isotope fractionation constants ($^{33/34}\epsilon$ and $^{13}\epsilon$) and non-mass-dependent fractionation constant (^{33}E).

^{32}J	^{33}J	^{34}J	^{13}J	$^{33}\epsilon$	$^{34}\epsilon$	^{33}E	$^{13}\epsilon$
$(\times 10^{-8} \text{ molecule s}^{-1})$				$(\%)$			
1.283	1.278	1.284	1.249	-3.7 ± 4.5	1.1 ± 4.2	-4.2 ± 6.6	-26.8 ± 4.3

composition of volatile organic sulfur compounds such as dimethyl sulfide (DMS) were measured and negative $\delta^{34}\text{S}$ values were observed (Oduro et al., 2011). Negative $\delta^{34}\text{S}$ values in DMS would produce oceanic OCS more depleted in ^{34}S than 18 ‰ estimated by Krouse and Grinenko (1991). Hence, the estimated $\delta^{34}\text{S}$ values in OCS of 11 ‰ (Krouse and Grinenko, 1991) also should be reconsidered. Therefore, in the future, high precision determinations of the sulfur isotopic composition atmospheric OCS are needed to confirm both whether $\delta^{34}\text{S}$ value in OCS of 11 ‰ is correct and whether OCS can be the major source of background SSA.

3.7.3 Non-mass-dependent signatures in sulfate in the modern and Archean atmospheres

Although there are no reports of $\Delta^{33}\text{S}$ values in background SSA, polar ice core records of sulfate after stratospheric sulfate aerosols show initially positive $\Delta^{33}\text{S}$ values (Baroni et al., 2008), suggesting there is non-mass-dependent fractionation in stratospheric sulfur chemistry. SO_2 photolysis and photo excitation, and SO_3 photolysis have been suggested to cause the non-mass-dependent signature observed in sulfate aerosol (Savarino et al., 2003; Pavlov et al., 2005; Baroni et al., 2008). In this study, ^{33}E at 20 km altitude is $(-4.2 \pm 6.6)\%$, mass-dependent to within the error (Table 3), and this is also consistent with the OCS photolysis experiment in the laboratory (Lin et al., 2011). Thus, OCS photolysis at 20 km altitude cannot explain the often observed positive $\Delta^{33}\text{S}$ values in sulfate. Additionally, both $\delta^{34}\text{S}$ and $\Delta^{33}\text{S}$ have positive values in glacial sulfate resulting after a stratospheric volcanic eruption (Baroni et al., 2007), and this also suggests that OCS photolysis does not contribute sulfate after stratospheric volcanic eruption.

Non-mass-dependent fractionation is found in Archean sedimentary sulfide and sulfate, suggesting atmospheric origin of the anomalous fractionation (Farquhar et al., 2000). The reducing Archean atmosphere may have contained elevated levels of OCS (Ueno et al., 2009), and it is therefore interesting to test whether or not photolysis of OCS may cause non-mass-dependent fractionation. Our results demonstrate that OCS photolysis does not cause large non-mass-dependent fractionation in ^{33}S , and thus this can be ruled out as the source of the non-mass-dependent signatures seen in the geological record, in agreement with the prediction of

Lyons (2009) and laboratory experiment of OCS photolysis (Lin et al., 2011).

4 Conclusions

The main result of this study is that OCS photolysis at 20 km altitude is not expected to produce isotopic fractionation larger than ca. 5 ‰ in $^{34}\epsilon$. The results do not support the large isotopic fractionation predicted by Leung et al. (2002) and apparently observed by Collusi et al. (2004). Additionally, the small isotopic fractionation for OCS photolysis as well as the OCS sink reaction with OH indicates that OCS can be the major source of background SSA. Investigation of isotopic fractionations in OCS sink reactions with $\text{O}(^3\text{P})$ radicals, and high precision measurement of isotopic composition of OCS in atmosphere are needed in future studies. Finally, based on our measurements OCS photolysis is not responsible for the positive $\Delta^{33}\text{S}$ values observed in sulfate aerosols.

Appendix A

Correction of absorption cross sections

The samples used in this study contained small isotopic impurities. The effect of the impurities was corrected through the following procedure. First, the cross section (σ) of each isotopologue was recalculated from the measured cross section (σ^*) for isotopically-enriched samples by simultaneously solving the following set of Eqs. (A1) to (A3):

$$^{32}\sigma^* = 0.99989 \ ^{32}\sigma + 0.00001 \ ^{33}\sigma + 0.0001 \ ^{34}\sigma \quad (\text{A1})$$

$$^{33}\sigma^* = 0.002 \ ^{32}\sigma + 0.9979 \ ^{33}\sigma + 0.0001 \ ^{34}\sigma \quad (\text{A2})$$

$$^{34}\sigma^* = 0.001 \ ^{32}\sigma + 0.0001 \ ^{33}\sigma + 0.9989 \ ^{34}\sigma. \quad (\text{A3})$$

After determining $^{32}\sigma$, $^{33}\sigma$ and $^{34}\sigma$, the cross section for natural abundance OCS ($^{12}\sigma^*$) is calculated using the natural distribution of sulfur isotopes (^{32}S : 0.9504, ^{33}S : 0.0075, ^{34}S : 0.0421). Finally, $^{12}\sigma$ and $^{13}\sigma$ are calculated by simultaneously solving a set of Eqs. (A4) and (A5).

$$^{12}\sigma^* = 0.989 \ ^{12}\sigma + 0.011 \ ^{13}\sigma \quad (\text{A4})$$

$$^{13}\sigma^* = 0.01 \ ^{12}\sigma + 0.99 \ ^{13}\sigma. \quad (\text{A5})$$

In the calculations described above, we ignored OC³⁶S and multiply substituted isotopologues because of their low abundance.

Supplementary material related to this article is available online at:

<http://www.atmos-chem-phys.net/11/10293/2011/acp-11-10293-2011-supplement.zip>

Acknowledgements. We wish to thank M. Nakagawa and D. Mahler for assistance of experiments. For providing actinic flux data, we wish to thank C. McLinden. We are grateful for the valuable comments received from an anonymous referee and S. Ono. This work is supported by Global Environmental Research Fund (A-0904) of the Ministry of the Environment, Japan, and Grant in Aid for Scientific Research (S) (23224013) of Ministry of Education, Culture, Sports, and Technology (MEXT), Japan. The research also has received funding from the European Community's Seventh Framework Programme (FP7/2007-2013) under grant agreement number 237890 and the Danish Council for Independent Research – Natural Sciences. S. H. is supported by Grant in Aid for JSPS Research Fellows (DC1 (No. 22-7563)) and Global COE program “Earth to Earths” of MEXT, Japan. Y. U. is supported by NEXT project of MEXT, Japan.

Edited by: J. Kaiser

References

- Barkley, M. P., Palmer, P. I., Boone, C. D., Bernath, P. F., and Suntharalingam, P.: Global distributions of carbonyl sulfide in the upper troposphere and stratosphere, *Geophys. Res. Lett.*, 35, L14810, doi:10.1029/2008gl034270, 2008.
- Baroni, M., Thiemens, M. H., Delmas, R. J., and Savarino, J.: Mass-Independent Sulfur Isotopic Compositions in Stratospheric Volcanic Eruptions, *Science*, 315, 84–87, doi:10.1126/science.1131754, 2007.
- Baroni, M., Savarino, J., Cole-Dai, J., Rai, V. K., and Thiemens, M. H.: Anomalous sulfur isotope compositions of volcanic sulfate over the last millennium in Antarctic ice cores, *J. Geophys. Res.*, 113, D20112, doi:10.1029/2008jd010185, 2008.
- Brenninkmeijer, C. A. M., Janssen, C., Kaiser, J., Röckmann, T., Rhee, T. S., and Assonov, S. S.: Isotope Effects in the Chemistry of Atmospheric Trace Compounds, *Chemical Reviews*, 103, 5125–5162, doi:10.1021/cr020644k, 2003.
- Castleman, A. W. J., Munkelwitz, H. R., and Manowitz, B.: Isotopic studies of the sulfur component of the stratospheric aerosol layer, *Tellus*, 26, 222–234, 1974.
- Chin, M. and Davis, D. D.: A reanalysis of carbonyl sulfide as a source of stratospheric background sulfur aerosol, *J. Geophys. Res.*, 100, 8993–9005, doi:10.1029/95jd00275, 1995.
- Colussi, A. J., Leung, F., and Hoffmann, M. R.: Electronic Spectra of Carbonyl Sulfide Sulfur Isotopologues, *Environ. Chem.*, 1, 44–48, doi:10.1071/EN04010, 2004.
- Crutzen, P. J.: The possible importance of CSO for the sulfate layer of the stratosphere, *Geophys. Res. Lett.*, 3, 73–76, doi:10.1029/GL003i002p00073, 1976.
- Danielache, S. O., Eskebjerg, C., Johnson, M. S., Ueno, Y., and Yoshida, N.: High-precision spectroscopy of ³²S, ³³S, and ³⁴S sulfur dioxide: Ultraviolet absorption cross sections and isotope effects, *J. Geophys. Res.*, 113, D17314, doi:10.1029/2007jd009695, 2008a.
- Danielache, S. O., Johnson, M. S., Nanbu, S., Grage, M. M. L., McLinden, C., and Yoshida, N.: Ab initio study of sulfur isotope fractionation in the reaction of OCS with OH, *Chem. Phys. Lett.*, 450, 214–220, doi:10.1016/j.cplett.2007.11.054, 2008b.
- Danielache, S. O., Nanbu, S., Eskebjerg, C., Johnson, M. S., and Yoshida, N.: Carbonyl sulfide isotopologues: Ultraviolet absorption cross sections and stratospheric photolysis, *J. Chem. Phys.*, 131, 024307, doi:10.1063/1.3156314, 2009.
- Farquhar, J., Bao, H. M., and Thiemens, M.: Atmospheric influence of Earth's earliest sulfur cycle, *Science*, 289, 756–758, 2000.
- Ferm, R. J.: The Chemistry Of Carbonyl Sulfide, *Chem. Rev.*, 57, 621–640, doi:10.1021/cr50016a002, 1957.
- Griffith, D. W. T.: Synthetic Calibration and Quantitative Analysis of Gas-Phase FT-IR Spectra, *Appl. Spectrosc.*, 50, 59–70, 1996.
- Hofmann, D. J.: Increase in the Stratospheric Background Sulfuric Acid Aerosol Mass in the Past 10 Years, *Science*, 248, 996–1000, doi:10.1126/science.248.4958.996, 1990.
- Hulston, J. R. and Thode, H. G.: Variations in the S³³, S³⁴, and S³⁶ Contents of Meteorites and Their Relation to Chemical and Nuclear Effects, *J. Geophys. Res.*, 70, 3475–3484, doi:10.1029/JZ070i014p03475, 1965.
- Johnson, M. S., Billing, G. D., Gruodis, A., and Janssen, M. H. M.: Photolysis of Nitrous Oxide Isotopomers Studied by Time-Dependent Hermite Propagation, *J. Phys. Chem. A*, 105, 8672–8680, doi:10.1021/jp011449x, 2001.
- Johnson, M. S., Feilberg, K. L., Hessberg, P. V., and Nielsen, O. J.: Isotopic processes in atmospheric chemistry, *Chem. Soc. Rev.*, 31, 313–323, 2002.
- Jørgensen, S., Grage, M. M. L., Nyman, G., and Johnson, M. S.: Isotope Effects in Photodissociation: Chemical Reaction Dynamics and Implications for Atmospheres, *Adv. Quantum Chem.*, 55, 101–136, doi:10.1016/S0065-3276(07)00207-9, 2008.
- Junge, C. E.: The formation of the stratospheric sulfate layer, *Tellus*, 18, 685–685, doi:10.1111/j.2153-3490.1966.tb00286.x, 1966.
- Junge, C. E. and Manson, J. E.: Stratospheric Aerosol Studies, *J. Geophys. Res.*, 66, 2163–2182, doi:10.1029/JZ066i007p02163, 1961.
- Kjellström, E.: A Three-Dimensional Global Model Study of Carbonyl Sulfide in the Troposphere and the Lower Stratosphere, *J. Atmos. Chem.*, 29, 151–177, doi:10.1023/a:1005976511096, 1998.
- Krouse, H. R. and Grinenko, V. A.: Stable Isotopes: NAACO, Scope, <http://www.icsu-scope.org/downloadpubs/scope43/index.html>, last access: July 2011, John Wiley and Sons, 1991.
- Leung, F.-Y. T., Colussi, A. J., Hoffmann, M. R., and Toon, G. C.: Isotopic fractionation of carbonyl sulfide in the atmosphere: Implications for the source of background stratospheric sulfate aerosol, *Geophys. Res. Lett.*, 29, 1474, doi:10.1029/2001gl013955, 2002.
- Liang, M.-C., Blake, G. A., and Yung, Y. L.: A semianalytic model for photo-induced isotopic fractionation in simple molecules, *J. Geophys. Res.*, 109, D10308, doi:10.1029/2004jd004539, 2004.
- Lin, Y., Sim, M. S., and Ono, S.: Multiple-sulfur isotope effects

- during photolysis of carbonyl sulfide, *Atmos. Chem. Phys.*, 11, 10283–10292, doi:10.5194/acp-11-10283-2011, 2011.
- Lyons, J. R.: Atmospherically-derived mass-independent sulfur isotope signatures, and incorporation into sediments, *Chem. Geol.*, 267, 164–174, doi:10.1016/j.chemgeo.2009.03.027, 2009.
- McLinden, C. A., McConnell, J. C., Griffioen, E., and McElroy, C. T.: A vector radiative-transfer model for the Odin/OSIRIS project, *Can. J. Phys.*, 80, 375–393, 2002.
- McLinden, C. A., Prather, M. J., and Johnson, M. S.: Global modeling of the isotopic analogues of N₂O: Stratospheric distributions, budgets, and the ¹⁷O-¹⁸O mass-independent anomaly, *J. Geophys. Res.*, 108, 4233, doi:10.1029/2002jd002560, 2003.
- Miller, C. E. and Yung, Y. L.: Photo-induced isotopic fractionation, *J. Geophys. Res.*, 105, 29039–29051, doi:10.1029/2000jd900388, 2000.
- Mills, M. J., Toon, O. B., Vaida, V., Hintze, P. E., Kjaergaard, H. G., Schofield, D. P., and Robinson, T. W.: Photolysis of sulfuric acid vapor by visible light as a source of the polar stratospheric CN layer, *J. Geophys. Res.*, 110, D08201, doi:10.1029/2004jd005519, 2005.
- Molina, L. T., Lamb, J. J., and Molina, M. J.: Temperature dependent UV absorption cross sections for carbonyl sulfide, *Geophys. Res. Lett.*, 8, 1008–1011, doi:10.1029/GL008i009p01008, 1981.
- Myhre, G., Berglen, T. F., Myhre, C. E. L., and Isaksen, I. S. A.: The radiative effect of the anthropogenic influence on the stratospheric sulfate aerosol layer, *Tellus B*, 56, 294–299, doi:10.1111/j.1600-0889.2004.00106.x, 2004.
- Notholt, J., Kuang, Z., Rinsland, C. P., Toon, G. C., Rex, M., Jones, N., Albrecht, T., Deckelmann, H., Krieg, J., Weinzierl, C., Binger, H., Weller, R., and Schrems, O.: Enhanced Upper Tropical Tropospheric COS: Impact on the Stratospheric Aerosol Layer, *Science*, 300, 307–310, doi:10.1126/science.1080320, 2003.
- Oduro, H., Kamysny Jr., A., Guo, W., and Farquhar, J.: Multiple sulfur isotope analysis of volatile organic sulfur compounds and their sulfonium precursors in coastal marine environments, *Mar. Chem.*, 124, 78–89, doi:10.1016/j.marchem.2010.12.004, 2011.
- Pavlov, A. A., Mills, M. J., and Toon, O. B.: Mystery of the volcanic mass-independent sulfur isotope fractionation signature in the Antarctic ice core, *Geophys. Res. Lett.*, 32, L12816, doi:10.1029/2005gl022784, 2005.
- Pitari, G., Mancini, E., Rizi, V., and Shindell, D. T.: Impact of Future Climate and Emission Changes on Stratospheric Aerosols and Ozone, *J. Atmos. Sci.*, 59, 414–440, doi:10.1175/1520-0469(2002)059<0414:IOFCAE>2.0.CO;2, 2002.
- Rothman, L. S., Jacquemart, D., Barbe, A., Chris Benner, D., Birk, M., Brown, L. R., Carleer, M. R., Chackerian, J. C., Chance, K., Coudert, L. H., Dana, V., Devi, V. M., Flaud, J. M., Gamache, R. R., Goldman, A., Hartmann, J. M., Jucks, K. W., Maki, A. G., Mandin, J. Y., Massie, S. T., Orphal, J., Perrin, A., Rinsland, C. P., Smith, M. A. H., Tennyson, J., Tolchenov, R. N., Toth, R. A., Vander Auwera, J., Varanasi, P., and Wagner, G.: The HITRAN 2004 molecular spectroscopic database, *J. Quant. Spectrosc. Ra.*, 96, 139–204, doi:10.1016/j.jqsrt.2004.10.008, 2005.
- Rudolph, R. N. and Inn, E. C. Y.: OCS Photolysis and Absorption in the 200- to 300-nm Region, *J. Geophys. Res.*, 86, 9891–9894, doi:10.1029/JC086iC10p09891, 1981.
- Savarino, J., Romero, A., Cole-Dai, J., Bekki, S., and Thiemens, M. H.: UV induced mass-independent sulfur isotope fractionation in stratospheric volcanic sulfate, *Geophys. Res. Lett.*, 30, 2131, doi:10.1029/2003GL018134, 2003.
- Schinke, R.: Photodissociation Dynamics, Cambridge Monographs on Atomic, Molecular and Chemical Physics, Cambridge University Press, Cambridge, 436 pp., 1993.
- Schmidt, J. A., Johnson, M. S., and Schinke, R.: Isotope effects in N₂O photolysis from first principles, *Atmos. Chem. Phys.*, 11, 8965–8975, doi:10.5194/acp-11-8965-2011, 2011.
- Selwyn, G. S. and Johnston, H. S.: Ultraviolet absorption spectrum of nitrous oxide as a function of temperature and isotopic substitution, *J. Chem. Phys.*, 74, 3791–3803, doi:10.1063/1.441608, 1981.
- Stevenson, D. S., Johnson, C. E., Collins, W. J., and Derwent, R. G.: The tropospheric sulphur cycle and the role of volcanic SO₂, Special Publications, Geol. Soc. Lond., 213, 295–305, doi:10.1144/gsl.sp.2003.213.01.18, 2003.
- Suzuki, T., Katayanagi, H., Nanbu, S., and Aoyagi, M.: Nonadiabatic bending dissociation in 16 valence electron system OCS, *J. Chem. Phys.*, 109, 5778–5794, doi:10.1063/1.477200, 1998.
- Ueno, Y., Johnson, M. S., Danielache, S. O., Eskebjerg, C., Pandey, A., and Yoshida, N.: Geological sulfur isotopes indicate elevated OCS in the Archean atmosphere, solving faint young sun paradox, *P. Natl. Acad. Sci.*, 106, 14784–14789, doi:10.1073/pnas.0903518106, 2009.
- Watts, S. F.: The mass budgets of carbonyl sulfide, dimethyl sulfide, carbon disulfide and hydrogen sulfide, *Atmos. Environ.*, 34, 761–779, 2000.
- Weisenstein, D. K., Yue, G. K., Ko, M. K. W., Sze, N.-D., Rodriguez, J. M., and Scott, C. J.: A two-dimensional model of sulfur species and aerosols, *J. Geophys. Res.*, 102, 13019–13035, doi:10.1029/97jd00901, 1997.
- Wu, C. Y. R., Chen, F. Z., and Judge, D. L.: Temperature-dependent photoabsorption cross sections of OCS in the 2000–2600 angstrom region, *J. Quant. Spectrosc. Ra.*, 61, 265–271, 1999.